Modelling of rotational moulding process: analysis of process parameters and warpage on cycle times

A. Ianakiev* and K. K. Lim

The analysis of heat transfer in the rotational moulding process is a non-linear multi-dimensional matter, which involves a number of process conditions and thermal parameters. The present study mostly involves dimensional analysis, the changing effects of the process parameters and conditions on the process times for different processing circumstances. They have been explored and compared by using the two-dimensional slip flow model from Lim and Ianakiev.[1] The modelling helps to further identify and understand the dependence of the key thermal parameters due to external heating, external cooling, external–internal cooling and warpage on cycle times of the rotational moulding. In addition, the detail of the coincident node technique is discussed to present the key components of the conductivity matrix for an element 'abutting' a coincident node interface.

Keywords: Rotational moulding (rotomoulding), Heat transfer, Finite element method (FEM), Warpage, Coincident node technique

List of symbols

c	specific heat, J kg^{-1} K^{-1}
h	convective heat transfer coefficient, W m^{-2} K^{-1}
J	Jacobian matrix of coordinate transformation
k	thermal conductivity, W m^{-1} K^{-1}
N	shape function for finite element method t_{cy} cycle time, s
t_{ov}	heating (oven) time, s
T	temperature, K
T_a	internal air temperature, K
T_d	demoulding temperature, K
T_o	initial internal air temperature, K
T_{oc}	external temperature of forced cooling air, K
T_{ov}	oven temperature, K
ΔT	temperature difference between two media, K
δ	part thickness, m
ρ	density, kg m^{-3}
$II_1 = \frac{t_{ov}h_{ov}}{\rho_m c_m \delta_m}$	dimensionless heating time
$II_2 = \frac{t_{cy}h_{ov}}{\rho_m c_m \delta_m}$	dimensionless total cycle time
$II_3 = \frac{\rho_{p,l} c_{p,l} \delta_{p,l}}{\rho_m c_m \delta_m}$	plastic to mould thermal capacitance ratio
$II_4 = \frac{\rho_{P,mu} c_{p,mu} \Delta T_{p,mu}}{\rho_{p,l} c_{p,l} \Delta T_{p,l}}$	dimensionless latent heat per unit volume for plastic phase change
$II_5 = \frac{k_{p,l}}{\delta_p h_{ov}}$	dimensionless plastic conductance
$II_6 = \frac{k_m}{\delta_m h_{ov}}$	dimensionless mould conductance
$II_7 = \frac{T_d - T_{oc}}{T_{ov} - T_{oc}}$	dimensionless demoulding temperature
$II_8 = \frac{h_{ov}}{h_{oc}}$	external heating to cooling heat transfer coefficient ratio
$II_9 = \frac{h_{in}}{h_{oc}}$	internal air to external cooling heat transfer coefficient ratio
$II_{10} = \frac{h_{int}}{h_{oc}}$	warpage to external cooling heat transfer coefficient ratio

Subscripts

a	internal air
l	liquid phase of polymer
m	mould
p	polymer
s	solid phase of polymer
p	polymer
in	boundary of the inner polymer surface
mu	mushy phase of polymer
oc	cooling environment

School of Architecture, Design and Built Environment, Nottingham Trent University, Burton Street, Nottingham, NG1 4BU, UK

*Corresponding author, email anton.ianakiev@ntu.ac.uk

Published by Maney on behalf of the Institute
Received 26 January 2006; accepted 12 September 2007
DOI 10.1179/174328907X248221

ov heating environment
tc tacky phase of polymer
mu mushy phase of polymer
int boundary of the coincident node elements

Introduction

Rotational moulding is regarded as transient, high temperature, zero pressure and low shear. The final part is considered to be pressure free and stress free since the process does not utilise pressure to force the melt into a mould shape. The concept of rotational moulding originated from 'slush moulding' in the polyvinyl (PVC) manufacturing process. The technology was first developed in the USA in the 1940s before it was brought into the Europe in the 1950s.[2–4] Rotational moulding is ideal for a relatively short run production. It is regarded as of low processing cost in 100 000 to 300 000 parts per year range, and competes well with other plastic moulding processes through to 1 000 000 parts per year.[5] A rotomoulded part can be made as small as a doll's eye and as large as a 100 000 L storage tank.

The heating process of rotational moulding can be performed with various methods such as open flame heating, oven heating, internal air heating, molten salts, hot oil jacketed mould, infrared red or electrical heating. Among them, the oven heating method is the most popular today. In fact, the open flame heating method was first introduced to the rotational moulding industries in the early 1940s. However, it was gradually changed to the oven heating method owing to the latter one's conveniences; for example, cleanliness, health and safety and mould design flexibility.[6,7] Research by Kearn[6] shows that the open flame method helps to expedite the heating time but its overall cycle time is still longer than the oven heating method. This is the tradeoff between an effective heating time and a long cooling time, and it is also a reason why the oven heating is favoured over the open flame heating. The oven heating method was found, unfortunately, very inefficient since only 1·7% of the heat would go to the polymer. This is because the method requires the oven air to be heated up before heating the mould. Thus the oven heating method is relatively incompatible in energy saving.[6,7]

The applicable cooling methods for rotational moulding can be external air cooling (fan blowing), external internal air cooling, mist sprays, water showers, cold air jets and then spraying the moulds with water after a determined time and ambient air. Among them the fan blowing method is the most common cooling method used in the industry. Although the water spraying method helps to expedite the cooling, it is efficient only when the mould surface is hot enough ($\sim$100°C) to evaporate the spray. In rotational moulding, the heat transfer coefficient is commonly used to represent these heating and cooling methods. The coefficient is strongly dependent on the flow velocity, flow region, presence of turbulence, surface geometry and fluid properties such as dynamic viscosity, density and thermal conductivity.[8] Generally, the heat transfer coefficient can be assigned to a constant value or to vary with locations and time. The former approach for the modelling of the rotational moulding process can be found in papers.[9–11] The latter had also been adopted in rotational moulding model[12] by 'calibrating' the computer predicted results to fit with the experimental data from the process. In 1993, Sun and Crawford[13,14] studied the efficiencies of 1D internal heating and cooling effects with the ROHEAT program, in which the powder layers were treated as a packed bed (no mixing). The predicted results showed a considerable reduction in the process times.

Warpage is influenced by the magnitude of the temperature difference across the plastic, whereas the level of shrinkage is controlled by the rate of cooling.[15] However, part warpage can also be caused by inappropriate mould design and processing conditions such as rate of quench, excessive mould release agent, low internal mould pressure.[20] Warpage can be prevented if the shrinkage throughout the part is uniform, or the cooling rates on the inside and outside surfaces of the plastic are the same. Assuming an isothermal plastic phase change, Gogos *et al.*[11] developed a 1D theoretical heat transfer model due to external cooling to identify the key processing parameters on rotational moulding affecting warpage. In their model, the air gap is formed with a fixed thickness between the mould and the plastic part. According to Crawford,[16] the internal cooling could reduce the warpage and the mould pressurisation could speed up the sintering process of polymers. Any unbalanced mould pressurisation might still lead to an uneven part thickness and result in further warpage. A high mould pressure will create large forces that might blow the mould apart. The experimental results from Chen *et al.*[17] showed that the mould pressurisation has no detrimental effect on the mechanical behaviour of a polyethylene product produced by rotational moulding, and has no effect on the residual stresses either. In addition, the mould pressurisation also helps to remove bubbles and further consolidates the melt. Consequently, it can improve the material properties, for example up to a 25% increase in impact strength and 5% in tensile strength.[18]

Dimensional analysis can reduce the number of parameters in the studies of rotational moulding process. According to Kreith and Bohn,[19] the results obtained from this method are rather incomplete without experimental data. Unfortunately, experimental data for different physical quantities are often not available for rotational moulding. This is because the experimental methods to measure these data are costly and not practical. In the present paper, some new and Gogos *et al.*[10,11] dimensionless groups are used to study the physical, boundary and time conditions of rotational moulding system, quantitatively. The relationships of the key dimensionless groups in Gogos *et al.*[10] to rotational moulding have been evaluated by using various 1D numerical approaches. The evaluations assumed to be able to compensate for the lack of empirical data for comparisons at the present dimensional analysis. Consequently, this allows further use of the dimensionless groups for studying the effects of the external heating, external cooling, external–internal cooling and warpage on rotational moulding process.

Coincident node technique for warpage and slip flow modelling

With symmetrical cooling assumption only half the slip flow model from Lim and Ianakiev[1,22] is applied to the

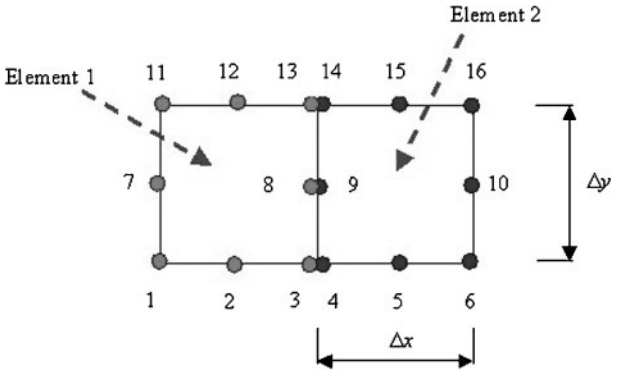

1 Structure of coincident node elements

cooling process. The details of the 2D slip flow model and the efficient algorithm for the non-isothermal phase changes can refer to the publications.[1,21] In the present paper, the coincident node technique[23] is used to numerically model the warpage in a slip flow model in order to simulate the thermal break of the continuum between the mould and polymer interface. The technique is an alternative to the thin element method. Presuming that a dimensional ratio aspect of the thin element area in Fig. 1 is $\Delta y/\Delta x=100$, the thin element technique was found at most to be 0·02% different from the results of the coincident node technique. Samonds *et al.*[24] pointed out that for a dimensional high aspect ratio of thin element area of $\Delta y/\Delta x=350$, there was only a 1·9% of mathematical difference between the coincident node technique and the thin element technique. This indicates that there should be very little difference in the numerical behaviour of these two methods.

Conveniently, the interface condition of the coincident elements may be imposed after the mesh has been designed, i.e. simply by adding coincident nodes along the internal surface. On the other hand, the thin element approaches requires less programming effort but the additional elements will result in significant computational effects. The terms of the thin element appear in the capacitance matrix [*C*], and the stiffness matrix [*K*], but a term only appears in the [*K*] matrix for the coincident node technique after finite element discretisation.[24] Importantly, the coincident node element does not have to be present at the entire interface boundary at all times in the slip flow model. In the worst case, the global matrices of the thin elements might be invariably ill conditioned, i.e. spurious numerical results occur, unless an extremely fine mesh is used for the solution.[25] From these viewpoints, the coincident node technique is adopted.

As depicted in Fig. 1, the coincident node elements formed by two nodes coincide at the same position; one from each interface of the two adjacent elements. According to the figure, the coincident node topology for these coincident elements can be presented in Table 1.

Table 1 Coincident node topology for coincident elements

Coincident element	Node										
1	1	3	13	11	2	8	12	7	4	14	9
2	4	6	16	14	5	10	15	9	3	13	8

The relationship between the interface elements[23] can be described by

$$[\underline{K}^{e}_{int}]=\sum_{i,j=1}^{cn_I}\int_{\Gamma_{int}}\left[h_{int}N_j\left(N_i-\frac{1}{2}N_g\right)\right]d\Gamma^{e}_{int} \quad (1)$$

where $i, j=1, 2, \ldots, cn_I$. The cn_I represents the total node on the interface of coincident elements Γ_{int}. The subscript g is the number of the node coincident with i, and the superscript e stands for an element. This integration is performed for the elements on both sides of the interface. Since the N_jN_g cross-term appears twice during the integration, this term has a factor of 1/2 in equation (1). The final elemental stiffness matrix $[\underline{K}^{e}]$ becomes

$$[\underline{K}^{e}]=[\underline{K}^{e}]+[\underline{K}^{e}_{int}] \quad (2)$$

The following demonstration is presented to exemplify some components of the conductivity matrix for an element 'abutting' a coincident node interface such as at the element nodes 3, 8 and 13 in Fig. 1. The following equation (3) represents the shape functions for a 2D eight noded rectangular element (serendipity family) in the present model

$$\begin{aligned}
N^{e}_1&=-\frac{1}{4}(1-\xi)(1-\eta)(1+\xi+\eta) \quad ;\\
N^{e}_5&=\frac{1}{2}(1-\xi^2)(1-\eta)\\
N^{e}_2&=-\frac{1}{4}(1+\xi)(1-\eta)(1-\xi+\eta) \quad ;\\
N^{e}_6&=\frac{1}{2}(1+\xi)(1-\eta^2)\\
N^{e}_3&=-\frac{1}{4}(1+\xi)(1+\eta)(1-\xi-\eta) \quad ;\\
N^{e}_7&=\frac{1}{2}(1-\xi^2)(1+\eta)\\
N^{e}_4&=-\frac{1}{4}(1-\xi)(1+\eta)(1+\xi-\eta) \quad ;\\
N^{e}_8&=\frac{1}{2}(1-\xi)(1-\eta^2)
\end{aligned} \quad (3)$$

The relationship of the shape functions for the coincident nodes in Fig. 1 is

$$N_3=N_4 \quad (4)$$

The coincident boundary Jacobian J_Γ, formed by node numbers 3, 8 and 13 is

$$\begin{aligned}
J_\Gamma(1,\eta)&=\left\{\left|\left(\sum_{j=3,8,13}\frac{\partial N_j}{\partial\eta}x_j\right)^2+\left(\sum_{j=3,8,13}\frac{\partial N_j}{\partial\eta}y_j\right)^2\right|\right\}^{1/2}\\
&=|J_{int}|
\end{aligned} \quad (5)$$

Solving equation (1) gives

$$\begin{aligned}
K^{|e}_{3-3,int}&=\int_{-1}^{1}h_{int}N_3N_3|J_{int}|d\eta=\frac{4h_{int}|J_{int}|}{15}\\
K^{e}_{3-4,int}&=-K^{e}_{3-3,int}
\end{aligned} \quad (6)$$

where J_Γ is the coincident boundary Jacobian formed by node numbers 3, 8 and 13.

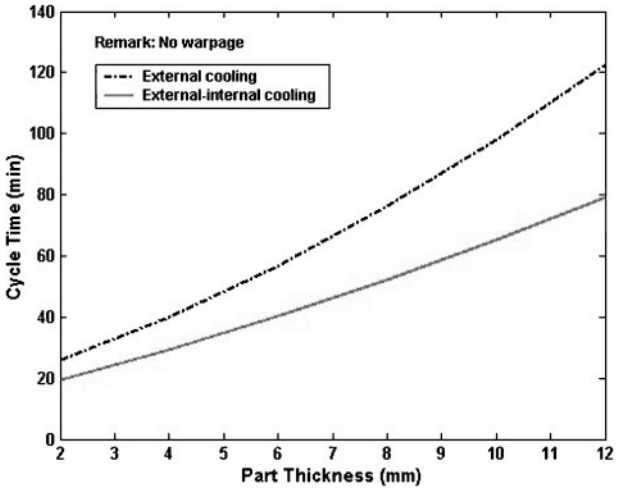

2 Comparisons of cycle times between external cooling and external–internal cooling processes for unwarped part

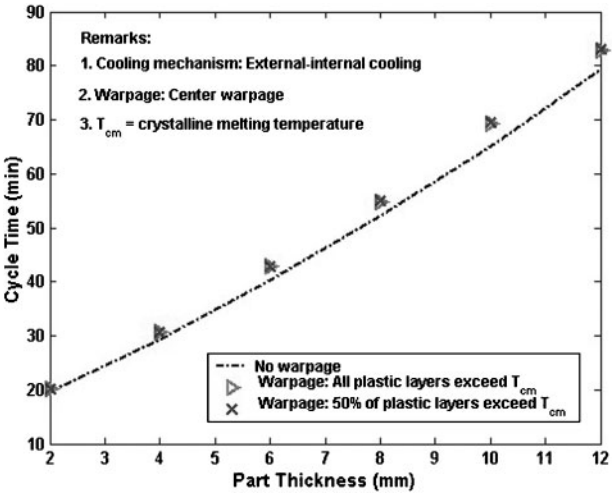

4 Comparisons of cycle times between warped and unwarped problems for external–internal cooling process

Results and discussion

The efficiency of coupling internal cooling into the rotational moulding process has been numerically studied and depicted in Fig. 2 for part thickness up to 12 mm. The results show that the external–internal cooling reduces significantly the cycle times particularly for the moulding of thick plastic products. According to Chen's offline experimental results,[20] the part warpage starts from the crystalline melting temperature T_{cm}. An early separation might be possible if an excess release agent used for the rotational moulding process.[15] The effects on cycle time due to this phenomenon, such as the onset of warpage at a different level of part solidity, have been plotted in Figs. 3 and 4 for the rotational moulding process with external cooling and external–internal cooling respectively. As expected in Fig. 3, the part warpage has reduced the efficiency of the external cooling. Interestingly the plot indicates that the cycle times due to the warpage for thin parts are independent of the degree of solidified part, which the warpage begins (i.e. early onset/late onset part warpage). The effect only becomes evident when the part thickness increases, for example the part thickness $\geqslant$8 mm. In contrast to the results, Fig. 4 shows that there are negligible differences in the cycle times between the early onset and late onset part warpage when the external–internal cooling method is applied to the rotational moulding process.

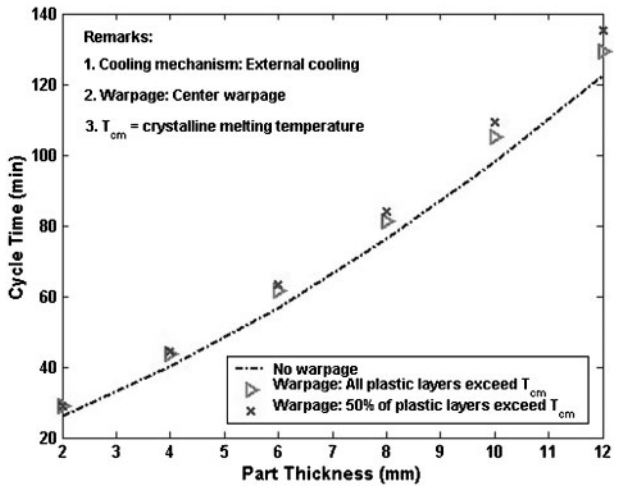

3 Comparisons of cycle times between warped and unwarped parts for external cooling process

The dimensionless plots of the 'base case' in the following Figs. 5–12 are constructed from the experimental data for the 4 mm part as given in Table 2. These figures demonstrate the influences of the key dimensionless process parameters resulted by different external processing conditions and/or warpage formation on the dimensionless heating time Π_1, as well as the dimensionless total cycle time Π_2. For similar cooling conditions, either external or external–internal cooling, all the dimensionless plots for the warped parts in general show a similar line pattern as their corresponding unwarped parts; Π_2 is shifted upwards approximately by a constant value for the dimensionless groups Π_3, Π_4, Π_5, Π_6, Π_9, and Π_{10}, and not by a constant value for the dimensionless groups Π_7, Π_8 and Π_9. The upward shifts of Π_2 due to warpage are comparatively small for the external–internal cooling method compared with the external cooling method. As a whole, Figs. 5–12 indicate that the external–internal cooling method for the rotational moulding is a more effective measure then the external cooling method to keep the cycle time short for the dimensionless groups Π_3 to Π_{10} (i.e. lower value of Π_2) respectively.

During the dimensional analysis, the variations of polymer related dimensionless groups (Π_3, Π_4 and Π_5) are only based on the selected phase change region that is appropriate (i.e. liquid phase – with subscript *l*). This is to keep the remaining dimensionless groups constant at the value corresponding to the base case. The selected region is a matter of study interest. The relationship between the dimensionless total cycle time Π_2, and the dimensionless groups of the polymer Π_3, Π_4 and Π_5 are plotted in Figs. 5*b*, 6*b* and 7*b* respectively. In these figures, the differences between Π_2 for the two different cooling methods could be larger if the thermal property variations for the warped or unwarped parts involve a wider temperature range to allow for the phase changes. Thus the cooling methods have considerable influence in enhancing the dimensionless group Π_2.

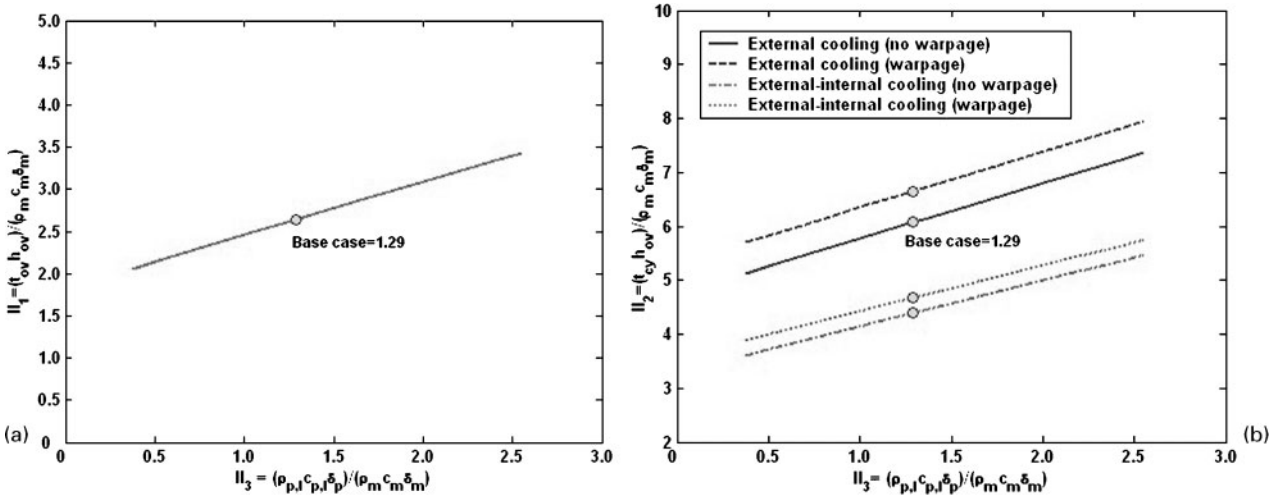

5 ***a*** **dimensionless heating time** Π_1 **and** ***b*** **dimensionless total cycle time** Π_2 **versus dimensionless plastics to mould thermal capacitance ratio** Π_3

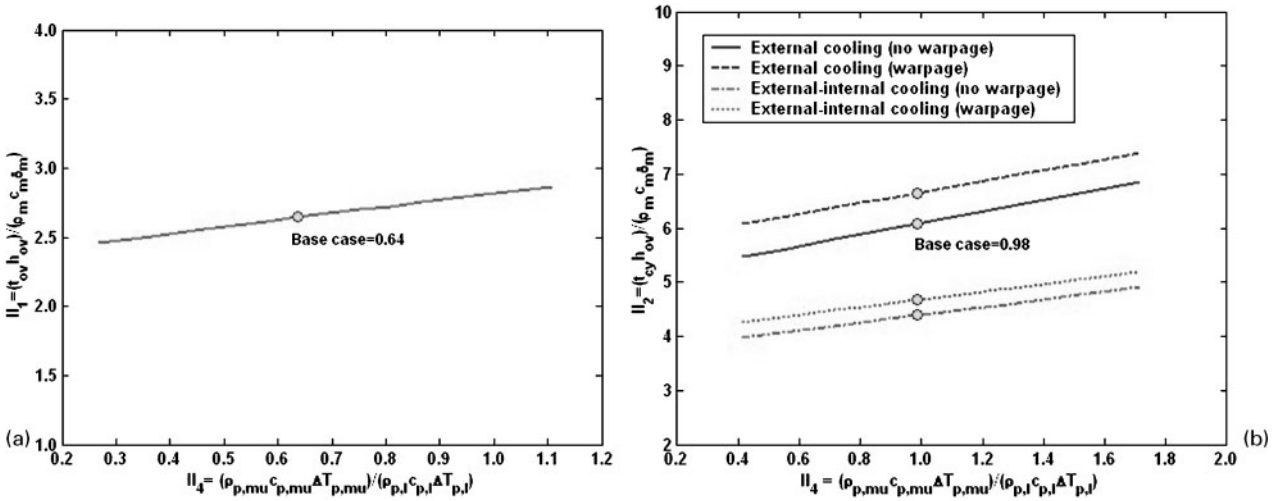

6 ***a*** **dimensionless heating time** Π_1 **and** ***b*** **dimensionless total cycle time** Π_2 **versus dimensionless latent heat per unit volume for plastic phase change** Π_4

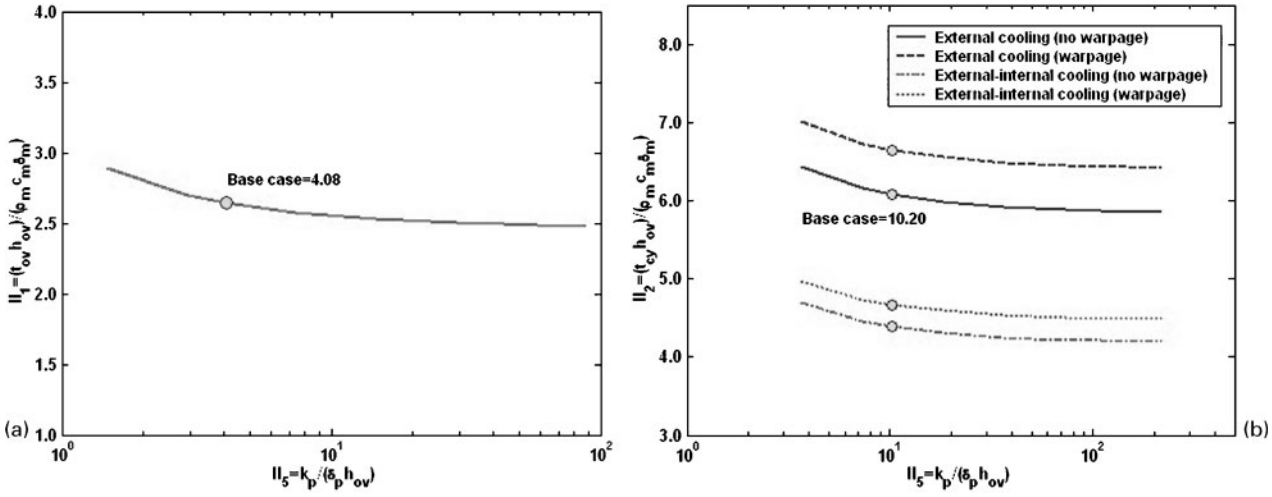

7 ***a*** **dimensionless heating time** Π_1 **and** ***b*** **dimensionless total cycle time** Π_2 **versus dimensionless plastic conductance** Π_5

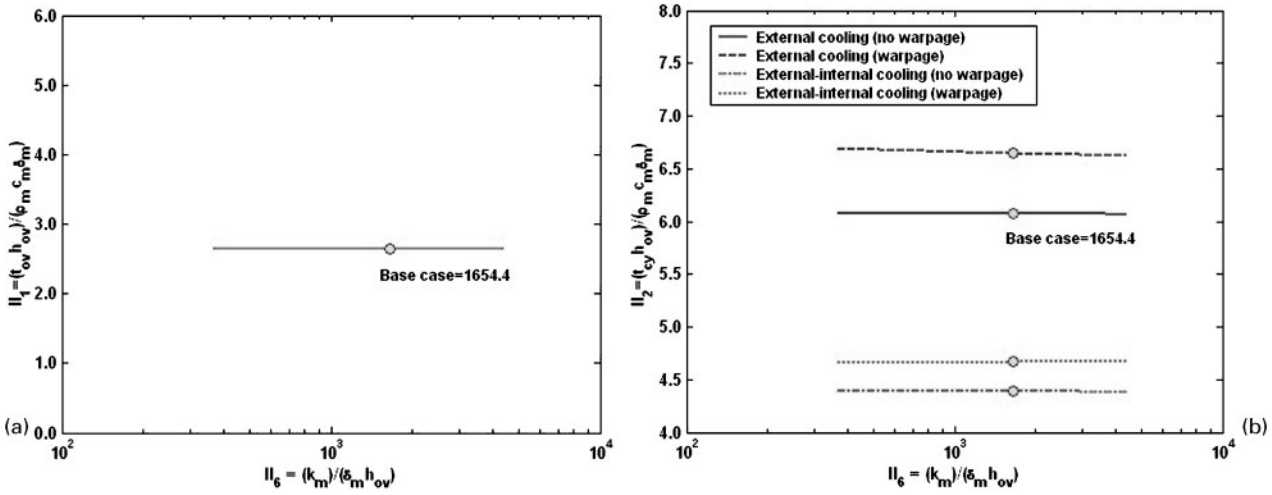

8 ***a*** **dimensionless heating time** II_1 **and** ***b*** **dimensionless total cycle time** II_2 **versus dimensionless mould conductance** II_6

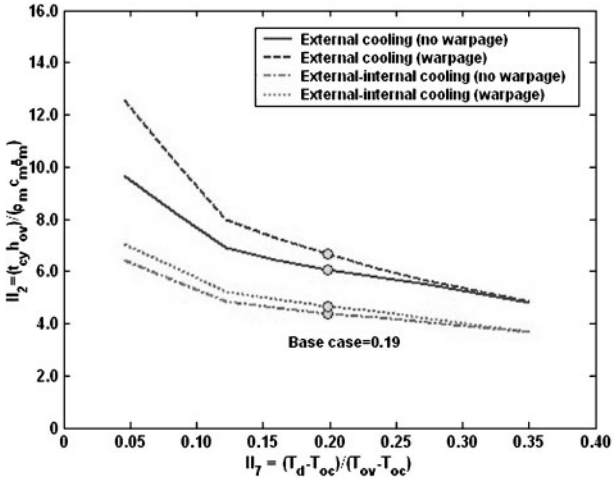

9 Dimensionless total cycle time II_2 **versus dimensionless demoulding temperature** II_7

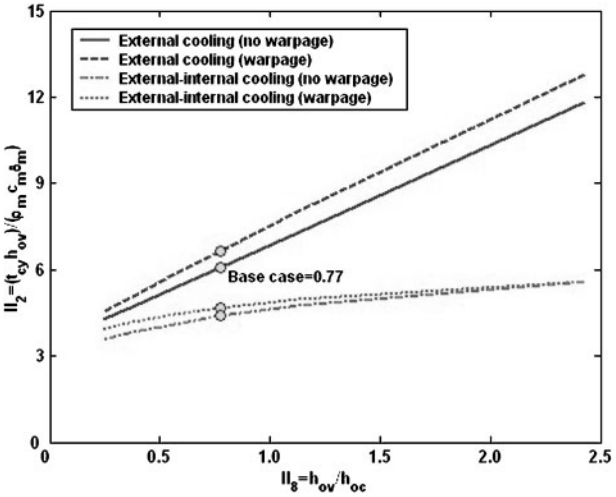

10 Dimensionless total cycle time II_2 **versus external heating to cooling heat transfer coefficient ratio** II_8

The magnitudes of II_3 represent the plastic to mould thermal capacitance ratio and II_4 represent the dimensionless latent heat per unit volume for plastic phase change. According to Figs. 5 and 6, the dimensionless heating time II_1, and dimensionless total cycle time II_2, increase linearly with the increasing II_3 and II_4 respectively. The magnitudes of II_4 indicate that II_1 and II_2 are dependent on the melting and crystallisation temperature ranges; the wider the phase change temperature the larger the values of II_4. Since II_4 represents the dimensionless latent heat of absorption or release per unit volume, any change in the latent heat for a phase change, a linear relationship between II_1 and II_4 (or II_2 and II_4) would be predicted from this dimensional relationship.

The plots from Fig. 7 illustrate that if the dimensionless plastic conductance II_5 is smaller than the base case, II_1 and II_2 increase moderately with decreasing II_5. When II_5 is larger than the base case, the values of II_1 and II_2 are almost approaching asymptotically. This suggests that any increase in the magnitude for the poor polymer thermal conductivity does not really improve the process times (heating time t_{ov} and total cycle time t_{cy}) of this pressure free rotomoulding process; as the thermal conductivity of the polymer does not vary appreciably for most polymers. According to Fig. 8, there is neither II_1 nor II_2 sensitive to the change in the dimensionless mould conductance, II_6. The capability of II_6 in expediting the process times is limited by the dimensionless group II_5 that is due to the poor thermal conductivity of the polymer. Thus the dimensionless group II_6 is regarded as a negligible factor for improving the heating and cooling times of a rotational moulding process.

The value of II_7 is a measure of the demoulding temperature. Its relationship to II_2 is plotted in Fig. 9. For II_7 smaller than the base case, i.e. decreasing the demoulding temperature T_d, the dimensionless cycle time II_2 increases moderately with decreasing II_7 for all the cooling circumstances. However, the continuous decreasing II_7 eventually results in a steep increase in II_2. At the stage, the effect of warpage has become more evident to deteriorate the dimensionless total cycle time, II_2, for the external cooling. For the external–internal cooling, however, the variation of II_2 is comparatively small between the warped and unwarped parts when there is a further decrease in II_7. This implies that external–internal cooling requires less additional cooling time to solidify warped products. It also indirectly implies that external–internal cooling can possibly

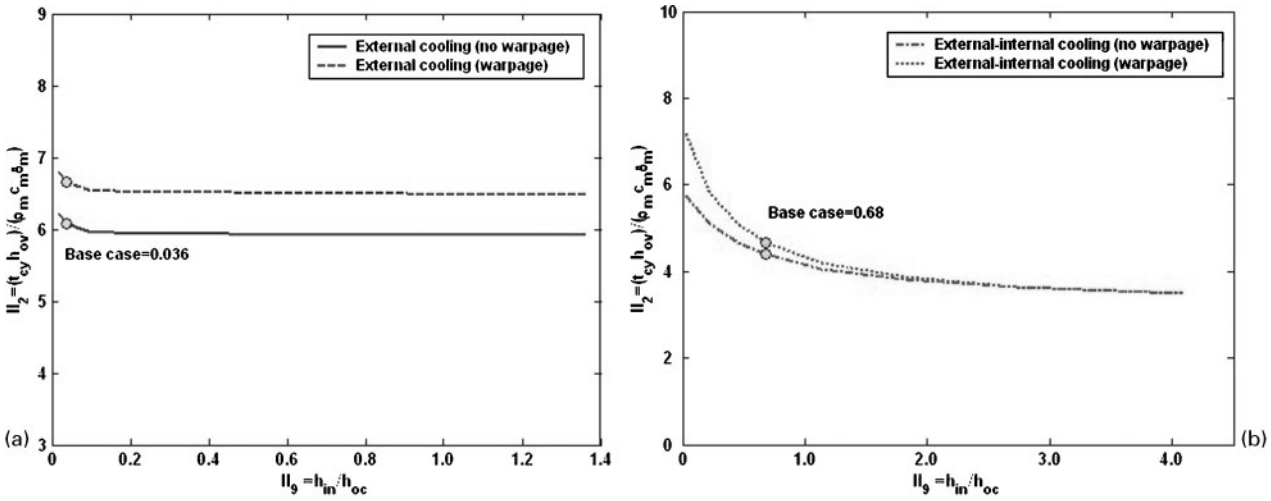

11 Dimensionless total cycle time II_2 versus internal air to external cooling heat transfer coefficient ratio II_9 for *a* external cooling and *b* external–internal cooling

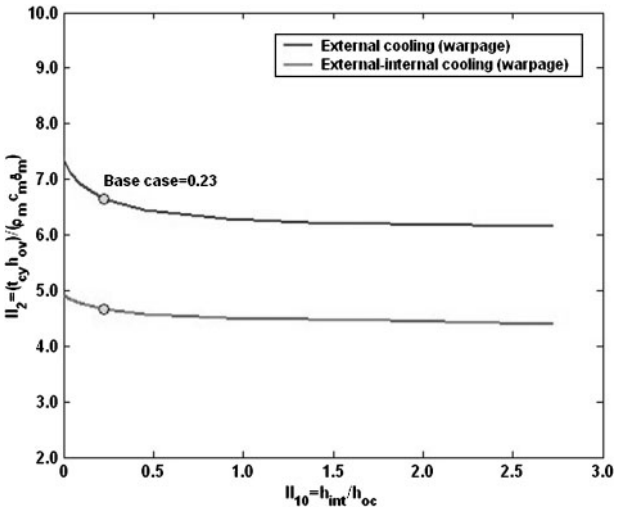

12 Dimensionless total cycle time II_2 versus air gap to external cooling heat transfer coefficient ratio II_{10}

prevent rotomoulder from producing 'too' under solidified parts even if the warpage could not be detected during the actual moulding process. So the external–internal cooling method is a promising technique to improve the cycle time and to maintain the quality of the final products. When the dimensionless demoulding temperature II_7 is larger than the base case, II_2 is no longer affected by warpage. This is because the warpage occurs a short time after the demoulding temperature is reached. The dimensionless cycle time II_2, however, is still influenced by the methods of cooling.

The curves in Fig. 10 show that the dimensionless total cycle time II_2 increases with increasing the dimensionless group II_8, representing the external heating to cooling heat transfer coefficient ratio. II_2 is significantly improved by the internal–external cooling method compared to the external cooling method especially when II_8 is larger than the base case. Generally the plots for the two side cooling (external–internal cooling) lack linearity; II_2 increases almost monotonically with increasing II_8 above the base case (corresponds to a decrease in h_{oc}). This is because the cooling process could still continuous from the internal plastic surface even at high a value of II_8. In contrast, II_2 for the one side cooling model (external cooling) is linearly sensitive to the change of II_8 for the warp and unwarped parts.

As shown in Fig. 11*a*, II_2 of the external cooling method is not sensitive to the magnitude of internal air to external cooling heat transfer coefficient ratio II_9, which corresponds to change in h_{in}. The dimensionless cycle time II_2 is influenced by h_{oc} which is inversely proportional to h_{in}. For the external–internal cooling method, Fig. 11*b* shows that decrease in II_9 from the base case leads to dramatic increase in II_2. For II_2 larger than the base case, however, II_9 is gradually becomes asymptotic. This implies that there is a limit for the cooling method to improve II_2, which is due to the poor thermal properties of the plastic. A large II_9 can be produced by increasing h_{in}; for example, by blowing high velocity air into the mould. However, this may potentially blow the mould apart when a high internal pressure builds up. In Fig. 12, the magnitude of II_{10} represents warpage to external cooling heat transfer coefficient ratio. The dimensionless total cycle time, II_2, is generally not sensitive to II_{10}. Thus the interface heat transfer coefficient for warpage h_{int} can be set to a constant value for warpage modelling of the rotational moulding process.

Table 2 Experimental process conditions of Enichem RP246H polymer in 'base case'

Process conditions of polymer RP246H (Ref. 12) in 'base case'				
δ_p, mm	T_o, °C	T_{ov}, °C	t_{ov}, min	t_{cy}, min
4	28·06	290	18·66	41·93

Conclusions

The numerical modelling shows that the onset of part warpage at different degree of part solidity does not affect the total cycle time for the rotational moulding process with external–internal cooling. For the external cooling only, the warpage formation for thicker parts does have a considerable influence on prolonging the

total cycle time. The dimensionless demoulding temperature II_7 shows that, at lower values of II_7 the internal–external cooling can help minimise possible warpage, when normally at this values of II_7 a warped part is produced under external cooling only. The external–internal cooling method improves the cycle time and maintains the quality of the final products. There is a limit for the internal cooling to improve further II_2 due to poor thermal properties of plastics. The dimensionless heating time II_1 and total cycle time II_2 are sensitive to dimensionless groups: plastic to mould thermal capacitance ratio II_3, dimensionless latent heat per unit volume for plastic phase change II_4, dimensionless demoulding temperature II_7, external heating to cooling heat transfer coefficient ratio II_8, and internal air to external cooling heat transfer coefficient ratio for external–internal cooling II_9; and they are insensitive to dimensionless groups: dimensionless plastic conductance II_5, dimensionless mould conductance II_6, internal air to external cooling heat transfer coefficient ratio for external cooling II_9, and warpage to external cooling heat transfer coefficient ratio II_{10}.

References

1. K. K. Lim and A. Ianakiev: Proc. ANTEC, Chicago, IL, USA, May 2004, SPE, 892–896.
2. D. Ramazzotti: Proc. SPE RETEC, October 1975, SPE, 43–63.
3. R. J. Crawford and J. L. Throne: 'Rotational molding technology', 315; 2001, Portland, William Andrew Inc.
4. G. L. Beall: 'Rotational molding – design, materials, tooling, and processing'; 1998, Munich, Hanser Publishers.
5. M. Narkis and N. Rosenzweig: 'Polymer powder technology'; 1995, Chichester, John Wiley & Sons.
6. M. P. Kearns, R. J. Crawford and N. Corrigan: Proc. ANTEC, Orlando, FL, USA, May 2000, SPE, 1360–1365.
7. M. J. Wright, A. G. Spence and R. J. Crawford: Proc. ANTEC, Toronto, Canada, April 1997, SPE, 3184–3188.
8. C. Long: 'Essential heat transfer'; 1999, Malaysia, Longman.
9. L. G. Olson, G. Gogos, V. Pasham and X. Liu: *Proc. ASME Heat Transf. Division*, 1997, **1**, 113–119.
10. G. Gogos, L. G. Olson, X. Liu and V. Pasham: *Polym. Eng. Sci.*, 1998, **38**, 1387–1397.
11. G. Gogos, L. G. Olson and X. Liu: *Polym. Eng. Sci.*, 1999, **39**, 617–629.
12. L. Xu: 'Prediction of the rotational moulding cycle', PhD thesis, Queen's University, 1996.
13. D. W. Sun and R. J. Crawford: *Plast. Rubber Process Appl.*, 1993, **19**, 47–53.
14. D. W. Sun and R. J. Crawford: *Polym. Eng. Sci.*, 1993, **33**, 132–139.
15. R. J. Crawford and K. O. Walls: SPE Topical Conference on Rotational Molding, Cleveland, OH, USA, 135–139; 1999, SPE.
16. R. J. Crawford: Proc. ANTEC, Atlanta, GA, USA, April 1998, SPE, 1108–1111.
17. C. H. Chen, J. L. White and Y. Ohta: *Polym. Eng. Sci.*, 1990, **30**, 1523–1528.
18. A. Spence: Proc. ANTEC, Atlanta, GA, USA, April 1998, SPE, 984–990.
19. F. Kreith and M. S. Bohn: 'Principles of heat transfer', 1986, New York, Harper & Row.
20. C. H. Chen, J. L. White and Y. Ohta: *Int. Polym. Process.*, 1991, **6**, 212–216.
21. K. K. Lim and A. Ianakiev: Proc. ANTEC, Chicago, IL, USA, May 2004, SPE, 897–901.
22. K. K. Lim and A. Ianakiev: *Polym. Eng. Sci.*, 2006, **46**, (7), 960–969.
23. M. Samonds: 'Finite element simulation of solidification in sand mould and gravity die castings', PhD thesis, University of Swansea, 1985.
24. M. Samonds, R. W. Lewis, K. Morgan and R. Symberlist: 'Computational techniques in heat transfer', Chapter 13; 1985, Swansea, Pineridge Press.
25. R. W. Lewis, W. K. Sze and H. C. Huang: *Int. J. Numer. Method Eng.*, 1988, **25**, 611–624.